

March 2020

INVESTIGATION OF TRACER-SURFACTANT-FOAM PROCESSES IN SHALLOW SUBSURFACE ENVIRONMENTAL REMEDIATION: HISTORY-MATCHING AND PERFORMANCE PREDICTION

Hazem Fleifel

Louisiana State University and Agricultural and Mechanical College

Follow this and additional works at: https://digitalcommons.lsu.edu/gradschool_theses



Part of the [Environmental Engineering Commons](#), and the [Petroleum Engineering Commons](#)

Recommended Citation

Fleifel, Hazem, "INVESTIGATION OF TRACER-SURFACTANT-FOAM PROCESSES IN SHALLOW SUBSURFACE ENVIRONMENTAL REMEDIATION: HISTORY-MATCHING AND PERFORMANCE PREDICTION" (2020). *LSU Master's Theses*. 5087.

https://digitalcommons.lsu.edu/gradschool_theses/5087

This Thesis is brought to you for free and open access by the Graduate School at LSU Digital Commons. It has been accepted for inclusion in LSU Master's Theses by an authorized graduate school editor of LSU Digital Commons. For more information, please contact gradetd@lsu.edu.

**INVESTIGATION OF TRACER-SURFACTANT-FOAM
PROCESSES IN SHALLOW SUBSURFACE ENVIRONMENTAL
REMEDATION: HISTORY-MATCHING AND PERFORMANCE
PREDICTION**

A Thesis

To be Submitted to the Graduate Faculty of the
Louisiana State University and
Agricultural and Mechanical
College in partial fulfillment of
the requirements for the degree of
Master of Science

in

The Craft and Hawkins Department of
Petroleum Engineering

by
Hazem Fleifel
B.S., University of Damascus, 2013
May 2020

ACKNOWLEDGEMENTS

I want to express my extreme thanks and respect to my thesis advisor Dr. Seung Ihl Kam of the Craft and Hawkins Department of Petroleum Engineering at Louisiana State University for his guidance throughout the development of this thesis. His critical thinking and thorough analysis inspired me and taught me how to not only organize myself but be a better engineer.

Also, I offer my deep appreciation and respect to my committee members, Dr. Ipsita Gupta, who provided valuable comments on this thesis, and Dr. Seung-Jong Jay Park for his generous advice and time.

This study is conducted through the support from the LSU Graduate School and collaborative efforts with Korea Rural Community Corporation (KRC) and Rural Research Institute (RRI). A generous donation of CMG STARS simulator from Computer Modeling Group made this study possible.

A special thanks goes to Mohammed Izadi, my research fellow. I could not have asked for a better person to become like a brother to me as he shared his advice and guidance.

I am indebted to Drs. Jerry and Sharon Weltman for encouraging me to apply to LSU and to pursue my master's degree. Without your help none of this would have happened. I also want to thank Dr. Anderw Wojtanowicz for helping me when I first came to LSU as a grad student.

I would like to thank my friends David Kekejian and Grigor Sargsyan from the Physics department, Younes Al-blooshi and Mozher Ibrahim for their help, encouragement and direction through several courses I have taken.

To my wife Oskinely Aguilera, I want to thank you for teaching me how to believe in myself and trust my instincts. With your inspiration, I feel I can achieve anything.

Finally, I want to express my immense gratitude to my brother, Said Flifl for his generous support, unconditional love, and unwavering belief in me to accomplish my goals.

TABLE OF CONTENTS

ACKNOWLEDGEMENTS.....	ii
LIST OF FIGURES.....	iii
ABSTRACT	v
1. INTRODUCTION	1
2. MOTIVATION AND OBJECTIVES	4
3. METHODOLOGY	7
4. RESULTS	11
Part 1. Homogeneous media with no oil	11
Part 2. Heterogeneous media without oil	15
Part 3. Heterogeneous media with oil	17
Part 4. Potential of follow-up foam processes	21
5. CONCLUSION	25
REFERENCES	26
VITA.....	29

LIST OF FIGURES

Figure 1. The field of interest in South Korea in this study: (a) three-dimensional topography map and (b) field map (about 0.6 km x 1 km) with concentration and distribution of contaminants (The green, yellow and red colors represent low, medium and high Concentration levels)	5
Figure 2. The site of interest for tracer/surfactant pilot test: (a) photo showing the site with injection, extraction, and monitoring wells and (b) areal layout with dimensions for simulation purpose	6
Figure 3. The grid system used for simulations showing the focus area (with finer grids) and the surrounding area (with coarser grids)	8
Figure 4. Injection condition from each of three wells: (a) during Day 1 and (b) during the entire period of pilot test (10 days)	10
Figure 5. Production history from the pilot tests: (a) effluent tracer (bromide) concentration, (b) effluent oil (xylene) concentration, (c) oil (xylene) saturation before the treatment, and (d) oil (xylene) saturation after the treatment (plots based on the original data from Um et al. (2013)).....	10
Figure 6. Bottom hole pressure responses from each of three wells: (a) during Day 1 and (b) during the entire period of pilot test (10 days) (see Fig. 4 for injection history)	11
Figure 7. Tracer concentration with time (during Day 1) at three different layers (top, middle, and bottom layers) (color scale in comparison with injection tracer mole fraction of 0.000151663)	12
Figure 8. Tracer concentration with time (during Day 2 through 9) at three different layers (top, middle, and bottom layers) (color scale in comparison with injection tracer mole fraction of 0.000151663)	13
Figure 9. Surfactant concentration with time (during Day 1) at three different layers (top, middle, and bottom layers) (color scale in comparison with injection surfactant mole fraction of 0.000059721)	13
Figure 10. Surfactant concentration with time (during Day 2 through 9) at three different layers (top, middle, and bottom layers) (color scale in comparison with injection surfactant mole fraction of 0.000059721)	14
Figure 11. Simulated production history of injected chemicals for homogeneous medium: (a) effluent tracer concentrations and (b) effluent surfactant concentrations from three extraction wells (north, south, and middle wells)	14

Figure 12 Introduction of heterogeneity in the system: (a) permeability distribution by using high-permeability (64 Darcy) and intermediate-permeability (16 Darcy) bands with low-permeability background (1/32 Darcy) and (b) resulting effluent tracer history from three extraction wells ($1 \text{ Darcy} = 10^{-12} \text{ m}^2$)	16
Figure 13. Tracer concentration with time (during Day 1) at three different layers (top, middle, and bottom layers) (color scale in comparison with injection tracer mole fraction of 0.000151663)	16
Figure 14. Tracer concentration with time (during Day 2 through 9) at three different layers (top, middle, and bottom layers) (color scale in comparison with injection tracer mole fraction of 0.000151663)	17
Figure 15. Tracer/surfactant-injection simulation results with oil density of 0.68 g/cc and viscosity of 0.7 cp: (a) effluent tracer concentration history and (b) effluent oil concentration history	18
Figure 16. Change in oil saturation with time at three different layers (layer 1, 2, and 10) with oil density of 0.68 g/cc and viscosity of 0.7 cp	19
Figure 17. Tracer/surfactant-injection simulation results with oil density of 1.0 g/cc and viscosity of 0.7 cp: (a) effluent tracer concentration history and (b) effluent oil concentration history	20
Figure 18. Change in oil saturation with time at three different layers (layer 1, 2, and 10) with oil density of 1.0 g/cc and viscosity of 0.7 cp	20
Figure 19. Tracer/surfactant-injection simulation results with oil density of 0.60 g/cc and viscosity of 0.7 cp: (a) effluent tracer concentration history and (b) effluent oil concentration history	21
Figure 20. Change in oil saturation with time at three different layers (layer 1, 2, and 10) with oil density of 0.60 g/cc and viscosity of 0.7 cp	21
Figure 21. Change in oil saturation with time for potential follow-up foam injection at the same total injection rate with 80 % gas fraction (MRF= 1, conventional gas-water injection (no foam) case)	22
Figure 22. Change in oil saturation with time for potential follow-up foam injection at the same total injection rate with 80 % gas fraction (MRF= 10, low-strength-foam case)	23
Figure 23. Change in oil saturation with time for potential follow-up foam injection at the same total injection rate with 80 % gas fraction (MRF= 100, high-strength-foam case)	23
Figure 24. Oil production from individual wells during foam injection: (a) MRF = 1, (b) MRF = 10, and (c) MRF = 100	24

ABSTRACT

In-situ subsurface remediation has been widely used as an efficient means of cleaning up non-aqueous phase liquid (NAPL) from contaminated soils and aquifer. The use of tracer, surfactant, and foam are often considered to keep track of the propagation of injected fluids in the medium, dissolve and mobilize contaminants trapped by capillary forces, and overcome the level of heterogeneity and improve displacement and sweep efficiencies.

This study shows an actual remediation process to reduce NAPL within a military base in South Korea, by injecting tracer and surfactant solutions together for a duration of 10 days. The site consists of 5 m by 5 m area with 3 m depth under the existing structure of fuel distribution facility. Computer simulation work is performed to match the history of produced tracer and oil concentrations from three extraction wells, by considering the nature of the heterogeneity in the site. With the characteristics of heterogeneity captured from the history match, this study further extends the scope to the use of foam remediation processes to examine how foam can reduce the mobility of injected gas phase and thus improve in-situ remediation.

1. INTRODUCTION

Since World War I, factories in the United States have manufactured chlorinated organic compounds and petroleum-based fuels, including tetrachloride (CT), trichloroethylene (TCE) and tetrachloroethylene (PCE). These synthetic chemicals have been widely used as solvents in numerous applications, for example, dry cleaning, textile manufacturing and grease removal. These organic compounds, however, have unfavorable effects on environment and human health (McCarty 2010). Of particular concern is groundwater contamination. Chemical organic components and petroleum-driven compounds such as benzene, toluene and xylene can drain underground from storage tanks and pipelines, and reach the groundwater table, causing severe widespread water contamination (Richter et al. 1986; Cherry et al. 1987; Gray 1993). These contaminants are commonly called non-aqueous phase liquid (NAPL). They can migrate through the vadose zone (or, unsaturated zone above ground water table) and be distributed as pools and/or residuals of oleic phases (Simpkin et al. 1999). Even though NAPL is immiscible with groundwater, it is still slightly soluble in water. There are two types of NAPLs: dense and light non-aqueous phase liquids (so-called DNAPLs and LNAPLs, respectively). Being denser than water, DNAPL tends to migrate deeper into the subsurface until it becomes trapped and accumulates on or near the impermeable boundaries (Simpkin et al. 1999). In contrast, being lighter than water, LNAPL tends to stay near the groundwater table, and spread and distribute between air and groundwater (Riser-Roberts 1998).

It is incumbent upon scientists and engineers to develop solutions to protect the underground aquifers from contamination, and come up with remedial actions to clean up the affected subsurface areas, if contaminated already. With limited successes, several technical solutions have been developed for remediation purposes, which are classified into two categories in general, *ex-situ* and *in-situ*. In *ex-situ* methods, the contaminated soils are hauled away and then treated off site. For example, a shallow subsurface of contaminated soils can be collected and then subjected to a bio-treatment, such as soil bacteria, in order to metabolize and convert the hydrocarbon molecules into harmless minerals (Alexanderson et al. 2014). In contrast, *in-situ* methods perform treatments on site, typically with injection, extraction and monitoring wells, without large-scale collection and transportation away from the field.

In-situ technologies can be categorized as either containment or treatment (Alleman et al. 2010). The containment technologies aim to prevent the contamination from spreading by walling

off the area by constructing thick walls around or immobilizing the contaminants by chemical reactions. The containment technologies may also construct hydraulic barriers by using water-injection or water-circulating wells, and the contaminated water is treated at the above-ground treatment facilities or down-hole filters installed along the well before re-injection/circulation back into the subsurface.

The other in-situ technology is treatment, with the goal of reducing the toxicity to a safer level satisfying the groundwater standards. There are many in-situ treatment technologies. For example, monitored natural attenuation mitigates the contamination through healing elements that naturally occur in the soil. It is a slow treatment process but can be combined with other active remediation techniques (Alleman et al. 2010). Bioremediation reduces toxicity by adding biological agents such as bacteria and microorganisms to modify the nature of contaminants and make it less severe (Shackelford and Jefferis 2000).

There are more active in-situ treatment technologies, sometimes called enhanced removal technologies. These include several methods, all of which involve injection and extraction procedures. One widely used application is soil flushing which reduces contamination by injecting a chemical into a well for cleaning underground purposes, and extracting the flushed liquid at the end of the process. The concept has been developed in many different ways especially to remove NAPLs. Among many, examples can be found in water injection to mobilize contaminant (Alleman et al. 2010; Abriola et al. 1995), surfactant injection to change the interfacial properties and/or dissolve organic contaminants (Abriola et al. 1995), and foam injection to improve mobility control (Lee and Kam 2014), overcome subsurface heterogeneity (Rosman and Kam 2009), or assist subsurface immobilization and stabilization of pollutants (Roostapour and Kam 2012; Roostapour et al. 2014). Surfactant/foam process (i.e., injecting surfactant solution as a pre-flush followed by foams) has long been recognized as an efficient means of diverting the flow into the low-permeable sections (Szafranski et al. 1997; Mamun et al. 2002). Polymer can be used together with these applications to modify profiles (Zhong et al. 2013).

In addition to remediation techniques, it is necessary to monitor the amount and distribution of contaminants in the subsurface before and after the treatments. Direct soil and groundwater sampling is one popular method, while tracer testing together with in-situ remediation is another common technique applied in the field. Tracers are chemical species that can partition (or, dissolve) into a certain phase selectively. Thus, by comparing injection history and production

history, information on the partitioning and non-partitioning phases in the subsurface can be estimated (Cooke 1971). Tracers can be used in single-well tests as well as inter-well tests to help the remediation process (Tang 1995; Jin et al. 1995).

2. MOTIVATION AND OBJECTIVES

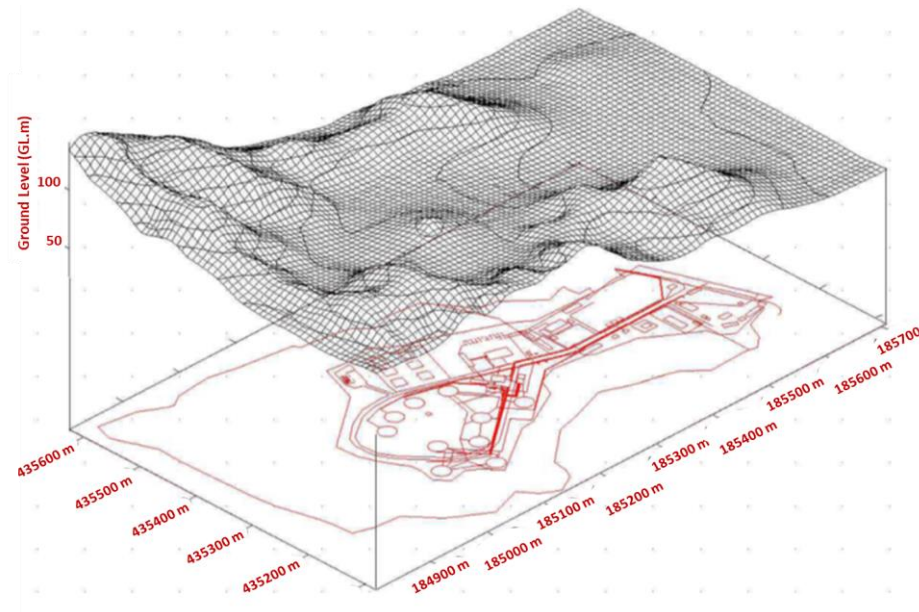
This study is motivated by a field case within a military base in South Korea (Si-Heung City, Gyeong-Gi Province). Fig. 1 shows the details of the field – three-dimensional topography map and its projection into the two-dimensional representation (Fig. 1(a)) and the concentration and distribution of the contaminants in the field measured by resistivity logs and oil/groundwater samples (Fig. 1(b)). The field has been contaminated by DNAPLs such as PCE and TCE as well as LNAPLs such as benzene, toluene, ethyl benzene and xylene (collectively referred to as BTEX), mainly leaked from storage tanks, distribution facilities and transportation pipelines. (Um et al. 2013).

The particular site of interest for tracer/surfactant pilot test in this study is near the center of the map in Fig. 1(b) where the contaminant concentration is relatively high (as colored in red). The site, concrete-covered and located within the fuel distribution facilities as shown in Fig. 2(a), has three injection wells and three extraction wells, with one monitoring well at the center, over the area of about 5 m x 5 m as shown in Fig. 2(b). The wells are about 3 m deep from the surface. Fluid injection is performed at pre-specified injection rates, and fluid extraction is performed with vacuum pumps on.

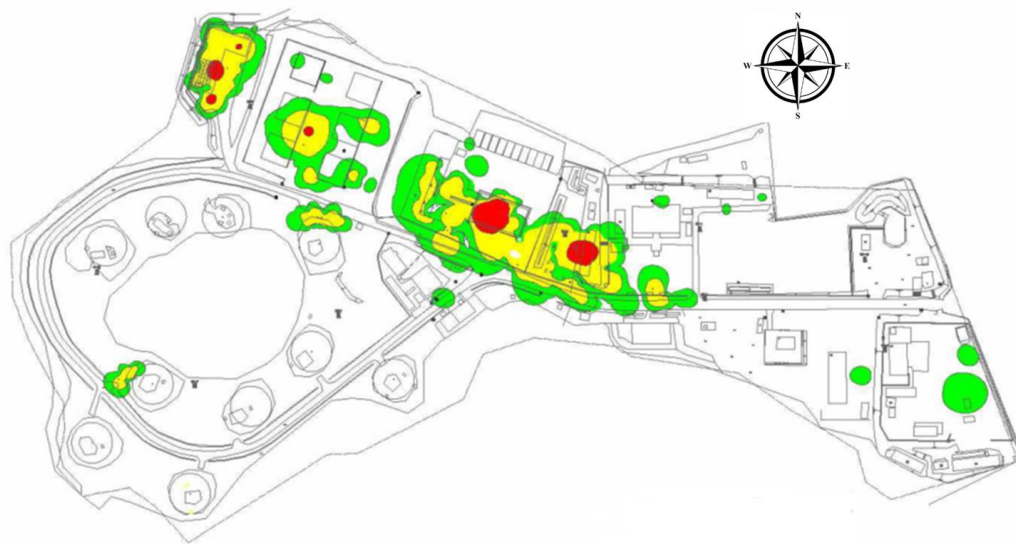
The concrete pavement, which is the top of the site, is considered as an impermeable seal. A field geological survey shows that the site has layers with sands and landfill near the top (less than 1 m shallow depth) and sands with silts and clays down below (down to 3 m depth), below which fresh rock exists as an impermeable boundary. The contaminant, which is a mixture of BTEX, has the average density of around 0.68 g/cc while the groundwater has the average density of around 1.04 g/cc. (Um et al. 2013).

The pilot test is carried out during 10 day period – each day with 9 hours of fluid injection followed by 15 hours of shut-in time (i.e., active field work only from 8 am through 5 pm daily, during which the site is available; otherwise classified as a restricted area due to military activities). While the surfactant solution is injected during the period at the same injection rate (i.e., $Q_w = 2.30 \text{ m}^3/\text{day}$ from each of the three injection wells), the tracer solution is injected during the first 200 minutes of Day 1 (i.e., $Q_w = 0.79 \text{ m}^3/\text{day}$ from each of the three injection wells). Bromide (Br^-) is used as a tracer, and Tween 80 (nonionic surfactant with concentration 0.1 - 0.2 %, far above its critical micelle concentration) is selected as a surfactant chemical for mobilization purpose (rather than solubilization) in the pilot test. After this pilot test

with tracer/surfactant injection, surfactant/foam process is planned to improve sweep efficiency. The entire process of using tracer, surfactant and foam, if successful, is viewed as a potential in-situ remediation solution to the entire field within the military base.



(a)

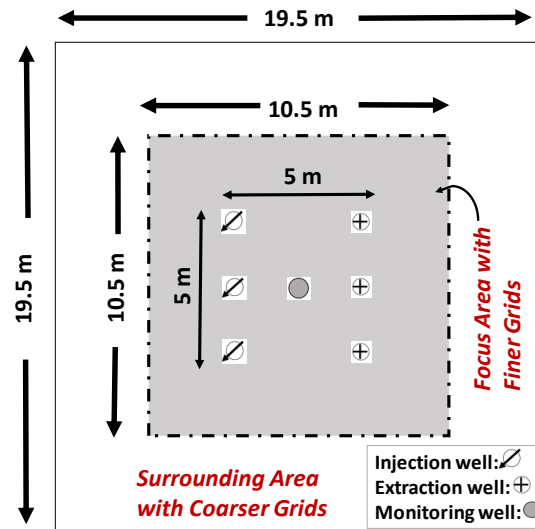


(b)

Figure 1. The field of interest in South Korea in this study: (a) three-dimensional topography map and (b) field map (about 0.6 km x 1 km) with concentration and distribution of contaminants (The green, yellow and red colors represent low, medium and high Concentration levels). Courtesy from Rural Research Institute, Korea Rural Community Corporation.



(a)



(b)

Figure 2. The site of interest for tracer/surfactant pilot test: (a) photo showing the site with injection, extraction, and monitoring wells (Courtesy from Rural Research Institute, Korea Rural Community Corporation) and (b) areal layout with dimensions for simulation purpose

Therefore, the objectives of this study are (i) to history-match the production of tracer and contaminant for the field pilot test and understand the pattern of heterogeneity in the field and (ii) to predict the effectiveness of follow-up surfactant/foam treatments based on foam characteristics.

3. METHODOLOGY

Computer simulations are conducted by using CMG STARS simulator, which solves partial differential equations for mass balance and energy balance. Assuming an isothermal process, the simulations deal mainly with material balance in terms of different components in the system such as water, gas, oil, surfactant and tracer (Lake et al. 1989), i.e.,

$$\begin{aligned} \frac{\partial}{\partial t} \left(\phi \sum_{j=1}^{N_p} \rho_j S_j \omega_{ij} + (1 - \phi) \rho_s \omega_{is} \right) + \nabla \cdot \left(\sum_j \rho_j \omega_{ij} \vec{u}_j - \phi S_j \vec{k}_{ij} \nabla \omega_{ij} \right) \\ = \phi \sum_{j=1}^{N_p} S_j r_{ij} + (1 - \phi) r_{is} \quad \text{for all } i \end{aligned} \quad (1)$$

where subscripts i, j and s represent components (such as tracer, surfactant, water, gas and oil), fluid phases (such as aqueous phase, gaseous phase and oleic phase), and solid phase (such as soil and rock), respectively. The terms such as ϕ , ω , ρ , S , \vec{u}_j , \vec{k}_{ij} , and r represent porosity, mass fraction, density, saturation, velocity (vector), dispersion coefficient (tensor), and reaction terms.

A grid system is built, as shown in Fig. 3, to encompass not only the focus area populated with three injection, three extraction (or production), and one monitoring wells (i.e., finer grids - 10.5 m x 10.5 m x 3 m system volume with 42 x 42 x 10 grid blocks; all seven wells fully perforated) but also the surrounding area (i.e., coarser grids - 19.5 m x 19.5 m x 3 m system volume with 39 x 39 x 10 grid blocks) applying no-flow boundary conditions. The bottom 9 grid layers (i.e., a total of 2.7 m thickness) are fully saturated with water (i.e., water saturation (S_w) = 1), while the uppermost top layer (0.3 m thickness) has water saturation (S_w) = 0.95 and gas (air) saturation (S_g) = 0.05. Note that this roughly captures the groundwater table of 0.3 m depth. The residual water and gas saturation in the unsaturated regions (S_{wr} and S_{gr} , respectively) are estimated to be 0.2 and 0.0, respectively. The site is reported to have the average oil saturation (S_o) of 0.05 (see the spatial distribution of oil below) and the residual oil saturation (S_{or}) of 0. (Um et al. 2013).

The relative permeability to each phase is expressed as follows (Lake et al. 1989):

$$k_{rw} = 0.79 \left(\frac{S_w - S_{wc}}{1 - S_{wc} - S_{or} - S_{gr}} \right)^{1.96} \quad (2)$$

$$k_{rg} = 1.00 \left(\frac{S_g - S_{gr}}{1 - S_{wc} - S_{or} - S_{gr}} \right)^{2.28} \quad , \text{and} \quad (3)$$

$$k_{ro} = (k_{row} + k_{rw}) (k_{rog} + k_{rg}) - (k_{rw} + k_{rg}) \quad (4)$$

where,

$$k_{row} = 0.9 \left(\frac{1 - S_w - S_g - S_{or}}{1 - S_{wc} - S_{or}} \right)^{2.12} \quad (5)$$

$$k_{rog} = 0.9 \left(\frac{1 - S_g - S_{wc} - S_{gr}}{1 - S_{wc} - S_{or} - S_{gr}} \right)^{2.12} \quad (6)$$

The subscripts w, o, and g represent aqueous, oleic and gaseous phases, respectively and k_{rw} , k_{ro} , and k_{rg} represent the relative permeabilities to individual phases.

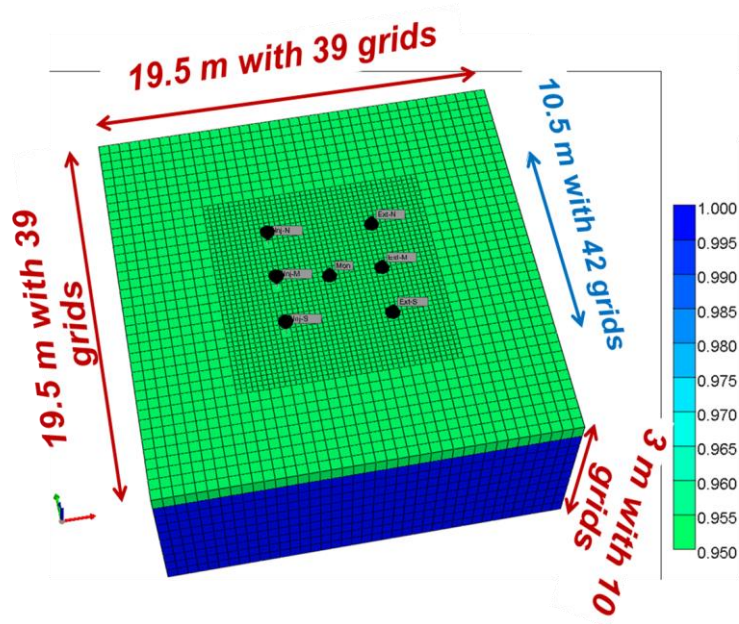


Figure 3. The grid system used for simulations showing the focus area (with finer grids) and the surrounding area (with coarser grids)

The site has the average absolute permeability (k) of 1.0 Darcy roughly (0.90 to 1.10 Darcy range) measured from the field pumping tests. The average porosity (\emptyset) is about 8.75%, relatively low compared to other unconsolidated sands because of compaction to make a stable building foundation. This study incorporates the highly heterogeneous aspect of the site into the distribution of absolute permeability (k), by keeping other parameters the same and uniform (\emptyset , S_{wr} , S_{or} , S_{gr} , k_{rw} , k_{ro} , k_{rg} , etc.).

The injection condition, as shown in Fig. 4, is continued for 10 days which is the duration of the pilot test. Each day consists of 9 hours of surfactant injection period (i.e., 8:00 am through 5:00 pm) at the liquid rate (Q_w) of around 2.30 m³/day from each of those 3 injection wells, followed by 15 hours of shut-in period. During the first 200 minutes of Day 1, an additional liquid rate (Q_w) of around 0.79 m³/day of the tracer solution is also injected simultaneously (this means the total liquid rate (Q_w) of 3.09 m³/day of tracer and surfactant solutions together). The bromide concentration of 671 mg/L and Tween-80 concentration of around 0.15 wt% are used in simulations, both based on the field groundwater. During the injection, three extraction wells are vacuum applied, which has the absolute pressure of 1 atm (or, 14.7 psia) approximately at the downhole condition, removing liquid inside the well efficiently. All numerical calculations are performed with the time step size (Δt) of 10 minutes. Note that the transport of each phase in subsurface porous medium can be expressed by Darcy's equation, for example,

$$Q_j = - \frac{k k_{rj} A \Delta P}{\mu_j L} \quad (7)$$

for phase j, where μ_j , ΔP , A and L represent viscosity of phase j, pressure drop, cross-sectional area, and length of the medium, respectively.

When air and surfactant solutions are injected together to investigate the effectiveness of foam process, the mobility of gas phase is reduced by MRF (or, mobility reduction factor), i.e.

$$Q_g = - \frac{k k_{rg} A \Delta P}{\mu_g MRF L} \quad (8)$$

and more details on foam modeling can be found from Kam and Rossen (2003).

Field pilot tests from Um et al. (2013) provide the results in terms of effluent bromide concentration (Fig. 5(a)) and effluent xylene concentration (Fig. 5(b)), as a function of time, and the change in oil saturation before and after the treatment (Figs. 5(c) and 5(d)). The xylene is used as a representative component for the oil phase, and the data points at the well locations are from the actual measurements (averaged over vertical distance). In flow simulations below with contaminants, the oil phase is assumed to be evenly distributed along the vertical distance, which is consistent with field observation.

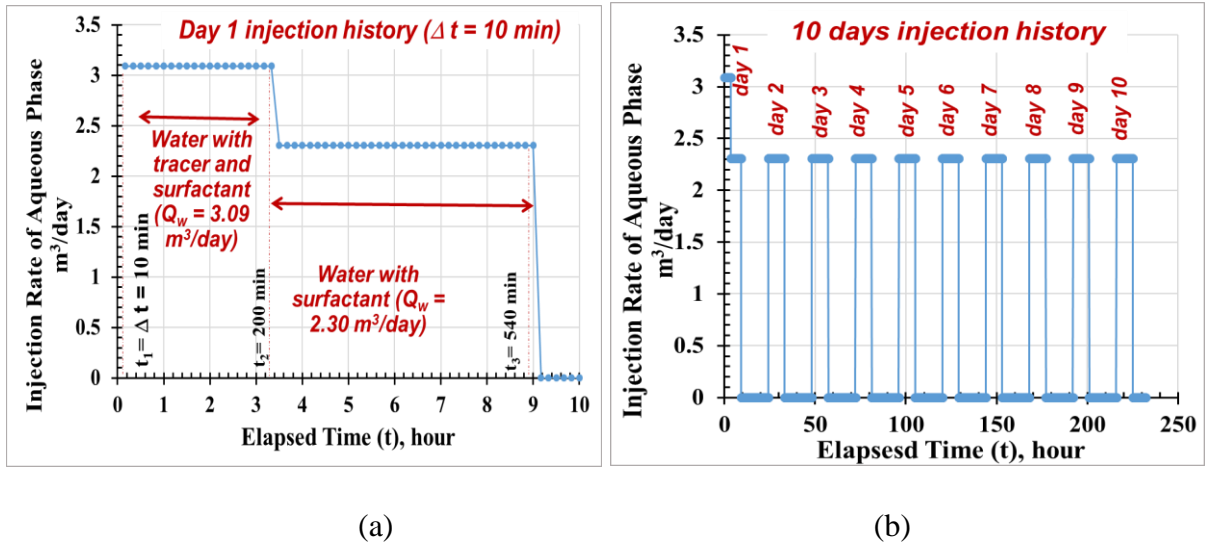


Figure 4. Injection condition from each of three wells: (a) during Day 1 and (b) during the entire period of pilot test (10 days)

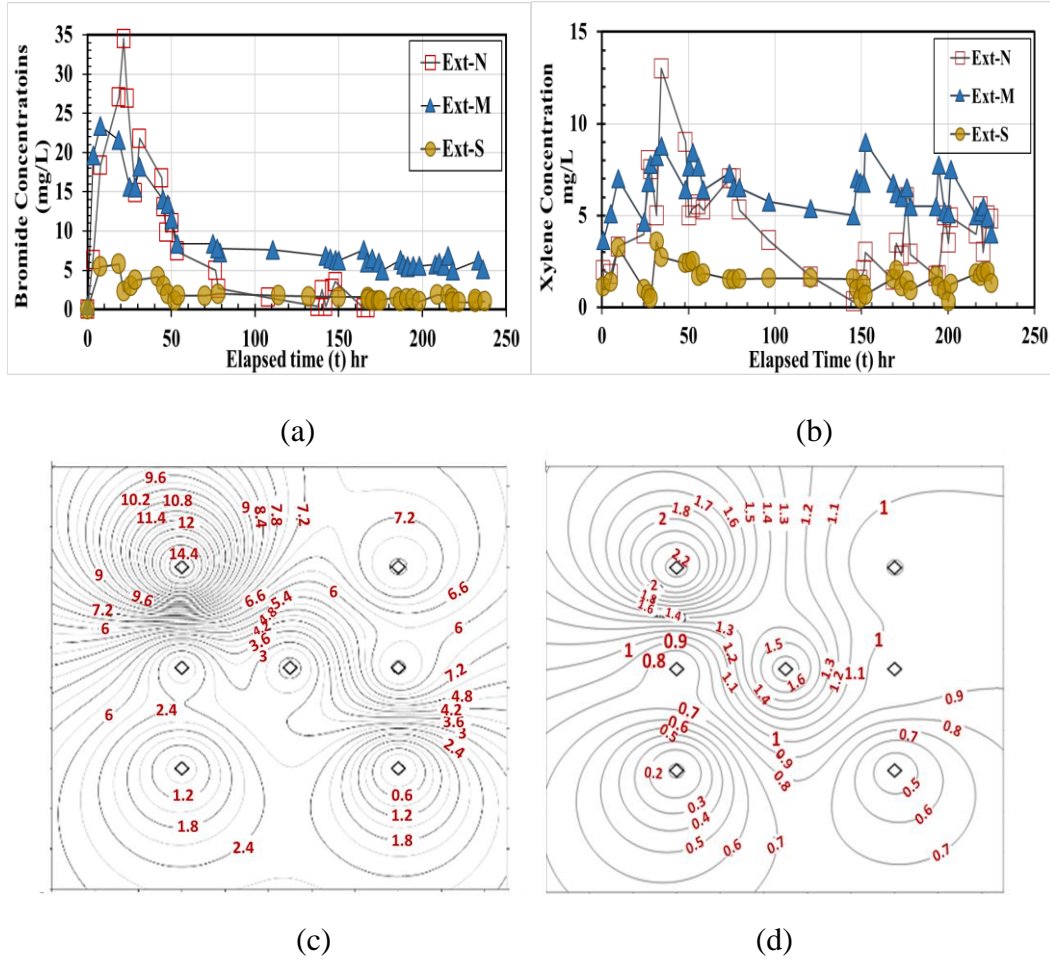


Figure 5. Production history from the pilot tests: (a) effluent tracer (bromide) concentration, (b) effluent oil (xylene) concentration, (c) oil (xylene) saturation before the treatment, and (d) oil (xylene) saturation after the treatment (plots based on the original data from Um et al. (2013))

4. RESULTS

The results of this simulation study are presented in a step-by-step manner, consisting of 4 different parts as follows:

- Part 1: Investigate tracer production history, assuming a homogeneous system with no oil;
- Part 2: Investigate tracer production history, assuming a heterogeneous system with no oil;
- Part 3: Investigate tracer and oil production history for the heterogeneous system; and
- Part 4: Investigate the potential of follow-up surfactant/foam processes.

The following sections examine each of these topics one by one.

Part 1. Homogeneous media with no oil

When the injection condition in Fig. 4 is applied to the system that has uniform permeability and porosity ($k = 1.0$ Darcy, $\phi = 8.75\%$), the corresponding changes in pressure from the three injection wells (north, south and middle) are calculated by the simulations as shown in Figs. 6(a) and 6(b). (Note that the vertical permeability is roughly a tenth of horizontal permeability, that is, $k_v = 0.10$ Darcy.) As expected from the system almost filled with water, the bottom hole pressure responds quickly to the change in injection rate. Because of symmetry, the pressure responses in the north and south wells are identical, while the middle well has a relatively high pressure because of its location (i.e., in between the north and south wells).

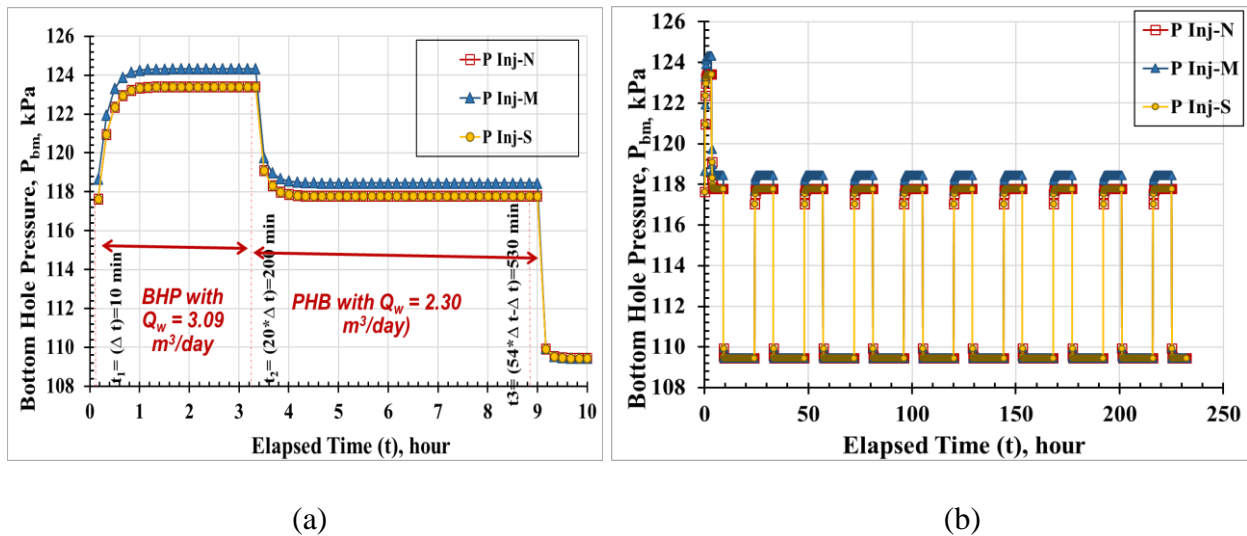


Figure 6. Bottom hole pressure responses from each of three wells: (a) during Day 1 and (b) during the entire period of pilot test (10 days) (see Fig. 4 for injection history)

The simulated tracer propagation during the pilot test is shown in Fig. 7 (Day 1) and Fig. 8 (Day 2 through 9) at three different vertical depths (grid layer 1 (top), 6 (middle), and 10 (bottom)). The injected tracer propagates radially during the first 200 minutes, beyond which tracer-free surfactant solution displaces the tracer bank further away from the wells forming ring-pattern tracer concentration in Day 1 (Fig. 7). In the following days, the ring pattern migrates further outwards making the rings bigger and tracer banks thinner and diluting out. Note that the tracer concentrations are all symmetric, and there is not much change along the vertical direction because of essentially no differences in terms of aqueous phase densities (i.e., ground water, tracer solution, and surfactant solution).

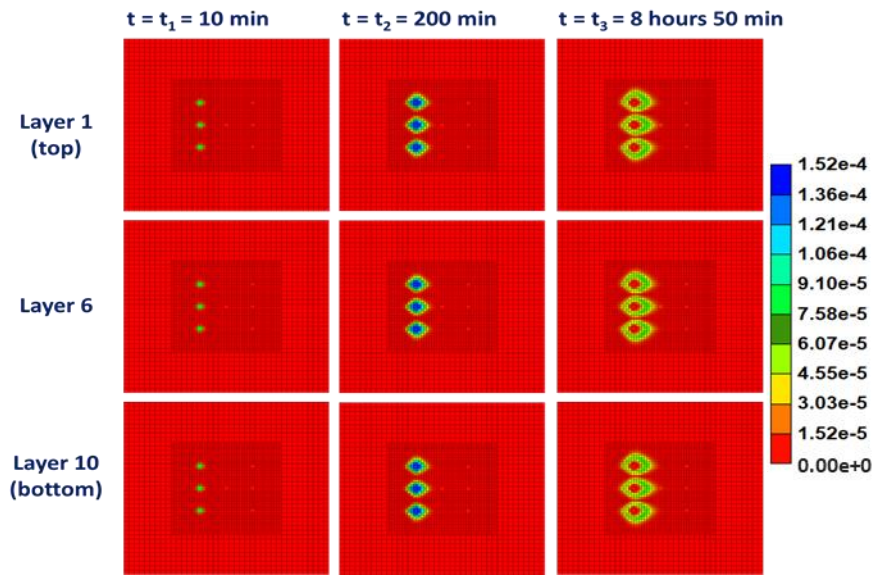


Figure 7. Tracer concentration with time (during Day 1) at three different layers (top, middle, bottom layers) (color scale mole fraction) (Injection mole fraction = 0.000151663)

Figs. 9 and 10 show similar results for surfactant chemicals. Because surfactant is injected throughout the injection period, its concentration is high at the well and decreases with radial distance. The symmetric nature of the pattern is also observed.

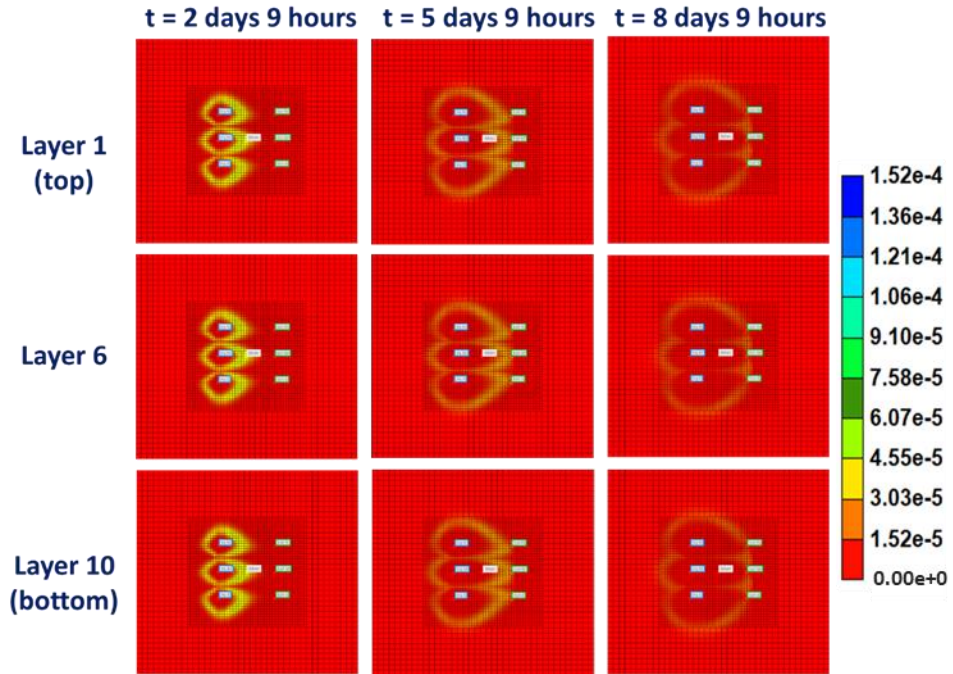


Figure 8. Tracer concentration with time (during Day 2 through 9) at three different layers (top, middle, bottom layers) (color scale mole fraction) (Injection mole fraction = 0.000151663)

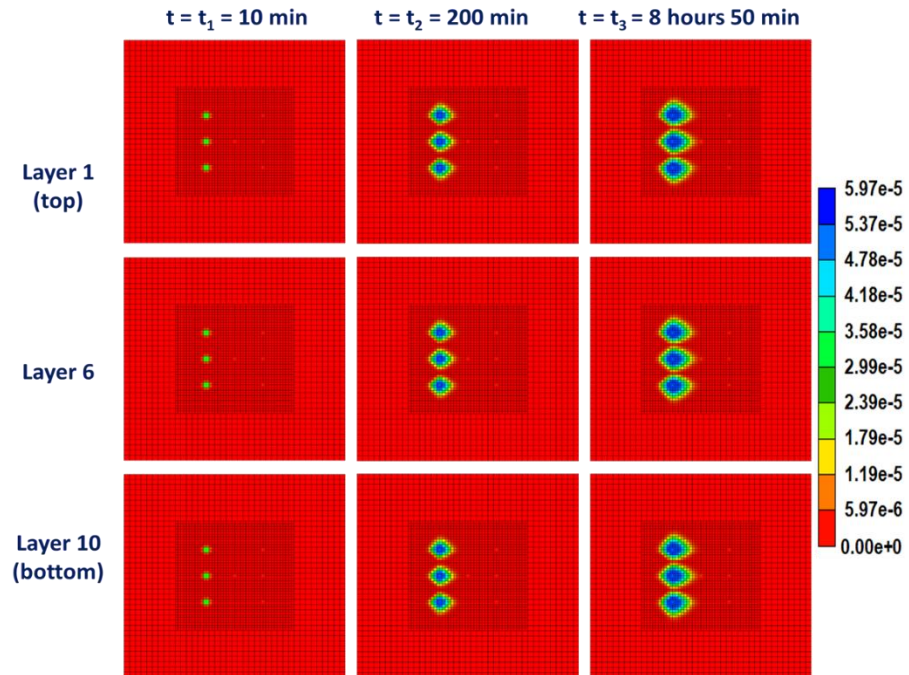


Figure 9. Surfactant concentration with time (during Day 1) at three different layers (top, middle, bottom layers) (color scale mole fraction) (Injection mole fraction = 0.000059721)

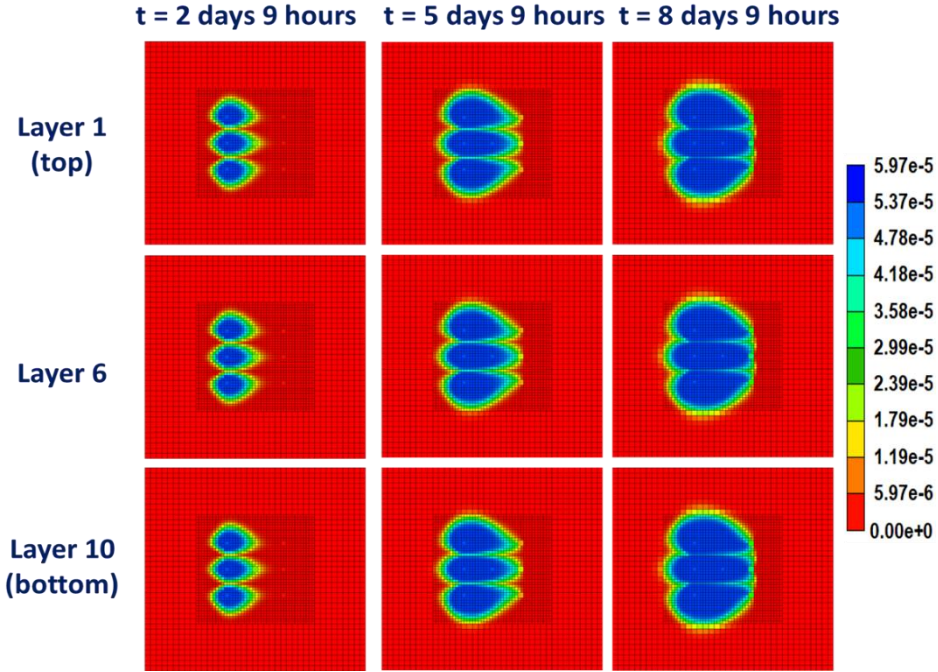


Figure 10. Surfactant concentration with time (during Day 2 through 9) at three different layers (top, middle, bottom layers) (color scale mole fraction) (Injection mole fraction = 0.000059721)

Figs. 11(a) and 11(b) show the effluent concentration of tracer and surfactant chemicals. When the tracer breaks through, the concentration keeps increasing until it reaches the peak, then decreases with long tails (Fig. 11(a)). This is consistent with the results in Figs. 7 and 8. On the contrary, surfactant concentration monotonically increases with time (Fig. 11(b)), which is also consistent with Figs. 9 and 10.

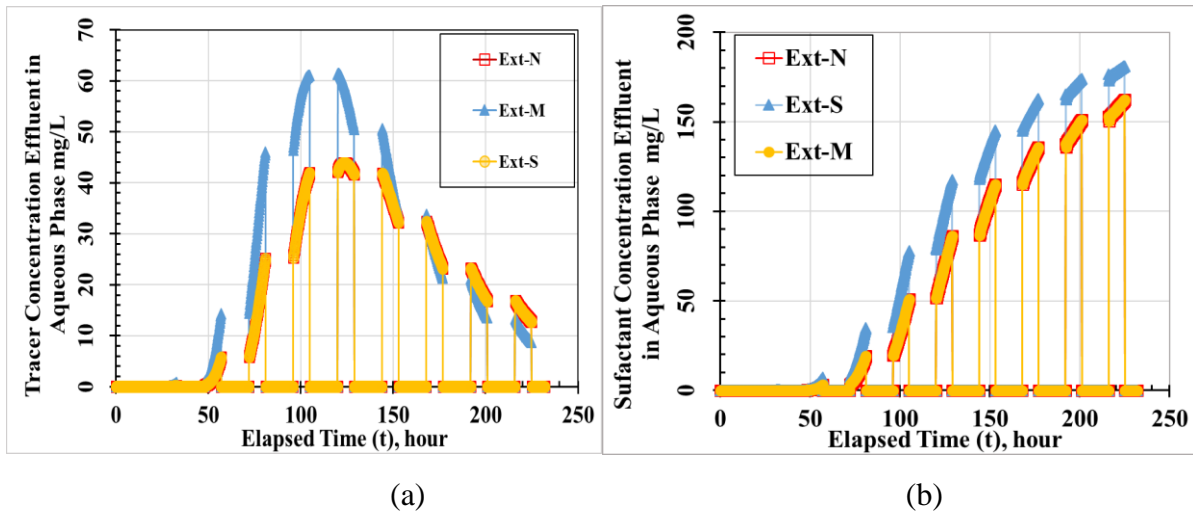


Figure 11. Simulated production history of injected chemicals for homogeneous medium: (a) effluent tracer concentrations and (b) effluent surfactant concentrations from three extraction wells (north, south, and middle wells)

Comparing the field tracer production history (Fig. 5(a)) with simulation results (Fig. 11(a)), there are significant differences between the two such as (i) field data showing no symmetry between the north and south wells and (ii) field data with earlier breakthrough time and peak time. They are caused by the heterogeneous nature of the site, which is investigated in the following sections.

Part 2. Heterogeneous media without oil

The tracer effluent history (Fig. 5(a)) in the field test shows a dramatic difference between north and south extraction wells. This section investigates possible patterns of areal distribution of absolute permeability to match the effluent history. Note k_v is a tenth of horizontal permeability (k) in all simulations below.

Comparing the tracer effluent histories from the homogeneous system (Fig. 11(a)) and from the field test (Fig. 5(a)) provides a few interesting differences. First, the results in the field tests (Fig. 5(a)) are not symmetric any longer such that the middle and north extraction wells have higher peaks, compared to the south extraction well. Second, although the peak sizes differ, there seems not much difference between the peak times in all three extraction wells (Fig. 5(a)). Third and last, the productions of tracer in all three extraction wells are much faster in Fig. 5(a) than Fig. 11(a). The first two aspects suggest (i) the presence of high-permeability paths in the system such that all three wells report the peaks at the similar times (implying high-permeability bands going from NW to SE direction) and (ii) a preferential tracer path from the north injection to north extraction wells. The third last aspect suggests that the system is highly heterogeneous with a low value of net-to-gross ratio (NTG) due to high clay contents (implying less area open to the active flow). These are confirmed by independent field survey and characterization study performed separately.

Based on more than 100 simulation runs (not shown), this study finds that one of the simplest ways to match the tracer effluent history is to use three permeability values (the high-permeability band (64 Darcy), which contains the intermediate-permeability band (16 Darcy) in it, is located within the low-permeability background (1/32 Darcy) with NTG = 0.333), as shown in Fig. 12(a). The corresponding tracer history is shown in Fig. 12 (b), which seems quite acceptable. Note that the bands are simply expressed by straight lines with similar widths. One may, of course, produce a tracer effluent history closer to Fig. 5(a) by considering more

sophisticated permeability variations from Fig. 12(a), and such a task, dealing with geostatistics and optimization, remains as a future assignment. Figs. 13 and 14 show the propagation of tracers for this system.

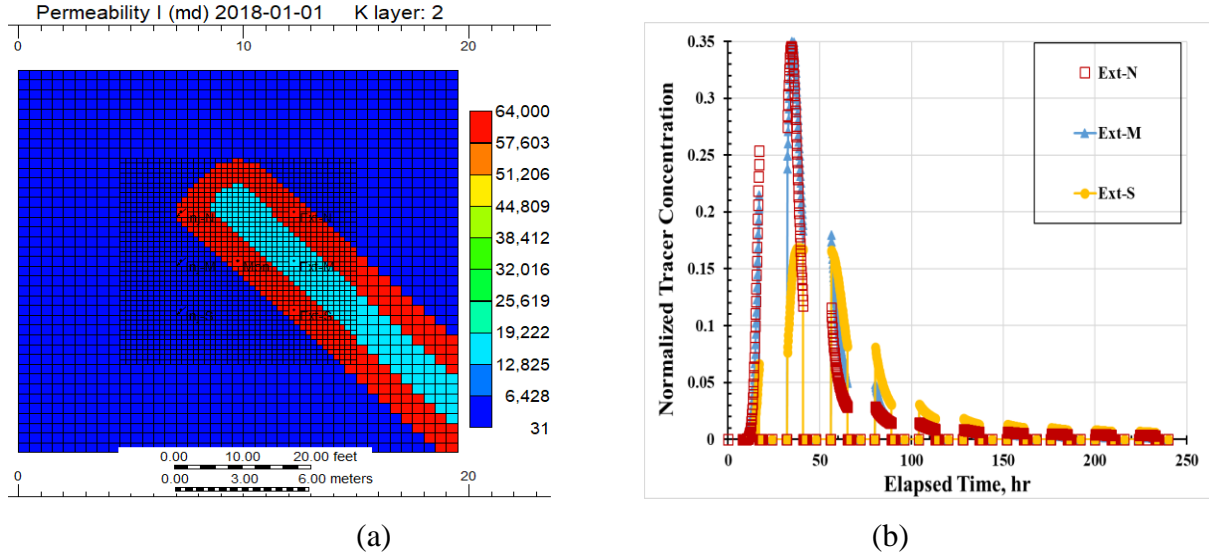


Figure 12. Introduction of heterogeneity in the system: (a) permeability distribution by using high-permeability (64 Darcy) and intermediate-permeability (16 Darcy) bands with low-permeability background (1/32 Darcy) and (b) resulting effluent tracer history from three extraction wells (1 Darcy = 10^{-12} m²)

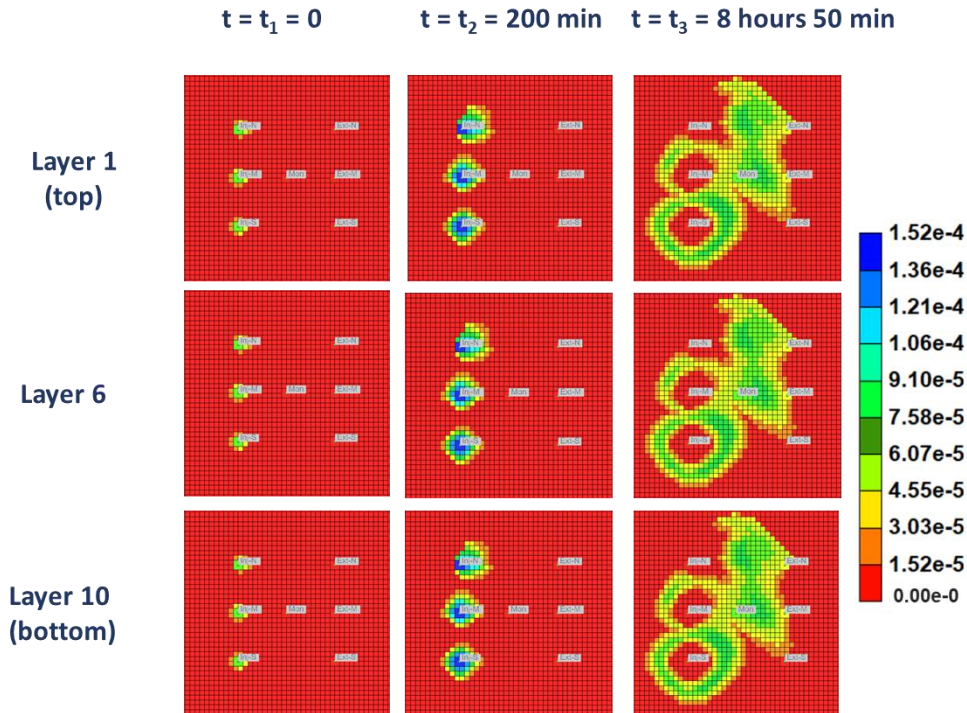


Figure 13. Tracer concentration with time (during Day 1) at three different layers (top, middle, bottom layers) (color scale mole fraction) (Injection mole fraction = 0.000151663)

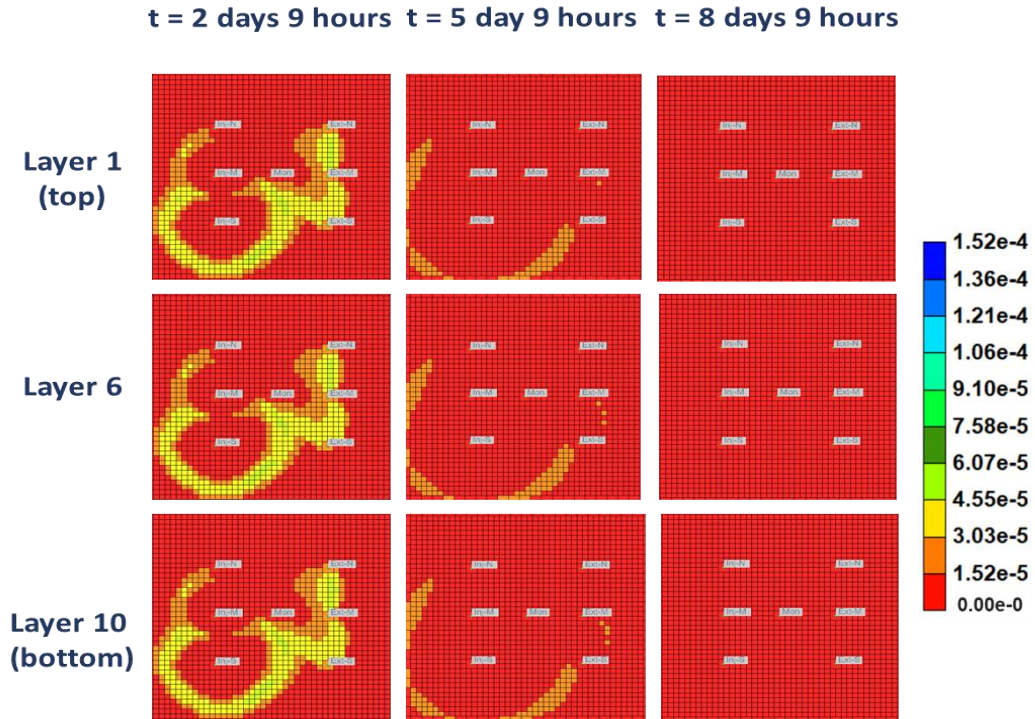


Figure 14. Tracer concentration with time (during Day 2 through 9) at three different layers (top, middle, bottom layers) (color scale mole fraction) (Injection mole fraction = 0.000151663)

It should be pointed out that the average permeability within the focus area containing three injection wells and three extraction wells is still the same as the field-reported value (~ 1 Darcy) (i.e., roughly 50% of the background area with $1/32$ Darcy and 50% area within bands with 32 Darcy (from 25% 64-Darcy high-permeability band and 25% 16-Darcy intermediate band)). This study does not claim that these three permeability values (64, 16, and $1/32$ darcies) are the best combination, even though they are selected based on more than 100 simulation runs – rather, they should be viewed as one of reasonable candidates to serve the purpose of this study.

(For example, other sets of permeability values such as (8, 2, $1/4$) and (16, 4, $1/8$), all in darcies, are also attempted to test different levels of heterogeneity but with less satisfactory tracer history.)

Part 3. Heterogeneous media with oil

On the top of the site map with permeability distribution (Fig. 12(a)), the contour map of oil saturation is imposed in order to investigate oil production history from the extraction wells, that is, oil concentration in the total fluids produced (Fig. 5(b)). Of course, the areal distribution of oil saturation before and after the treatment (Figs. 5(c) and 5(d)) is connected to the effluent oil

concentration (Fig. 5(b)) through material balance. This study uses the areal oil-saturation contours before the treatment (Fig. 5(c)) as an input, with the uniform oil distribution along the vertical direction as observed in the field due to high clay contents.

Although pure xylene has the density around 0.87 g/cc and the viscosity around 0.7 cp (Ciocirlan and Iulian 2009), the contaminant as an oil mixture in the field is reported to have a lower density at the similar viscosity. Fig. 15 presents simulation results showing the normalized tracer concentration (Fig. 15(a)) and the fraction of oil (Fig. 15(b)) that can be compared with Fig. 5(a) and Fig. 5(b), respectively, when the oil density of 0.68 g/cc and viscosity of 0.7 cp. Note that Fig. 15(a) shows slight changes compared to Fig. 12(b) because of the presence of oil in the media. Fig. 16 shows the change in oil saturation during tracer/surfactant injection at three different depths (first, second and tenth grid layers from the top). One can make two important observations. First, although the surfactant solution is injected uniformly along the entire vertical depth, the oil slowly rises upwards and accumulates near the top of the system (layer 1) when the surfactant solution is injected and disturbs the oil. And second, it is the layer 1 where most of the oil is swept by the injected surfactant solution and produced at the extraction wells.

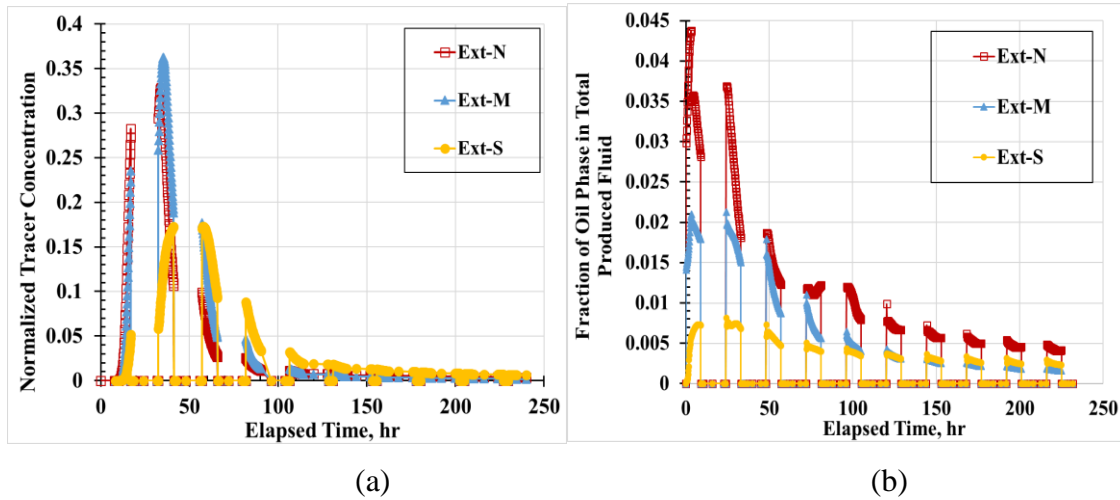


Figure 15. Tracer/surfactant-injection simulation results with oil density of 0.68 g/cc and viscosity of 0.7 cp: (a) effluent tracer concentration history and (b) effluent oil concentration history

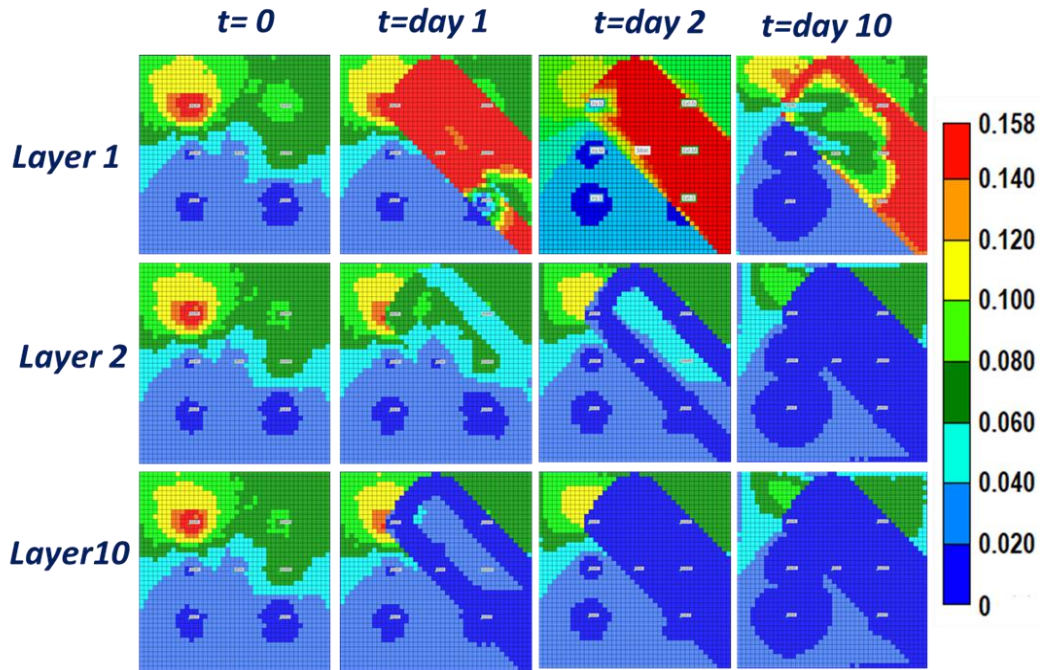


Figure 16. Change in oil saturation with time at three different layers (layer 1, 2, and 10) with oil density of 0.68 g/cc and viscosity of 0.7 cp (color scale showing oil saturation)

Two other cases are shown for different oil density values of 1.0 g/cm^3 and 0.60 g/cm^3 at the same oil viscosity of 0.7 cp, the results of which are shown in Figs. 17 and 18 as well as Figs. 19 and 20, respectively.

When the oil density is assumed to be 1.0 g/cm^3 , oil displacement pattern is similar in all depths because oil density is close to the density of surfactant solution (1.04 g/cm^3), as shown in Fig. 18. As a result, oil production from the south extraction well keeps increasing until about 8 days of surfactant injection.

When the oil density is assumed to be 0.60 g/cm^3 , oil migration to the top of the system is accelerated, and more oils are diverted into the middle extraction well (Fig. 20). As a result, oil production from the middle extraction is much higher at later time (i.e., $t > 3$ days).

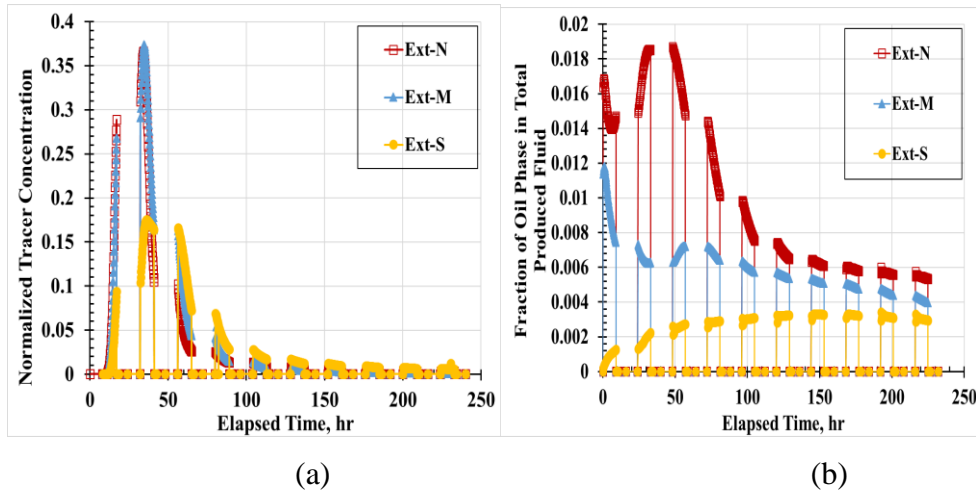


Figure 17. Tracer/surfactant-injection simulation results with oil density of 1.0 g/cc and viscosity of 0.7 cp: (a) effluent tracer concentration history and (b) effluent oil concentration history

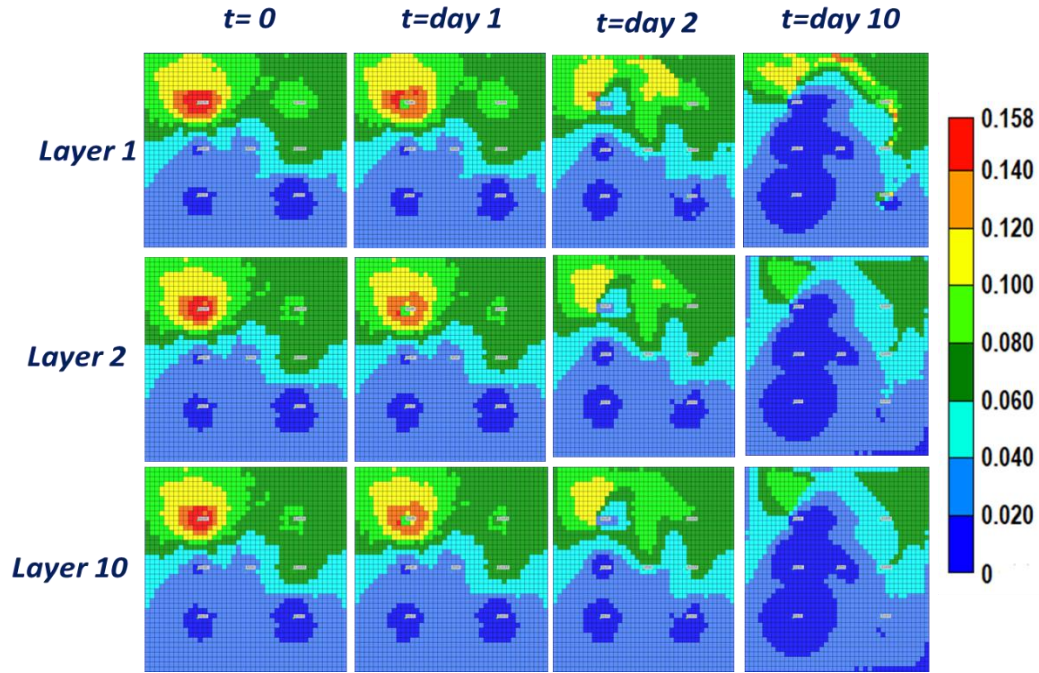
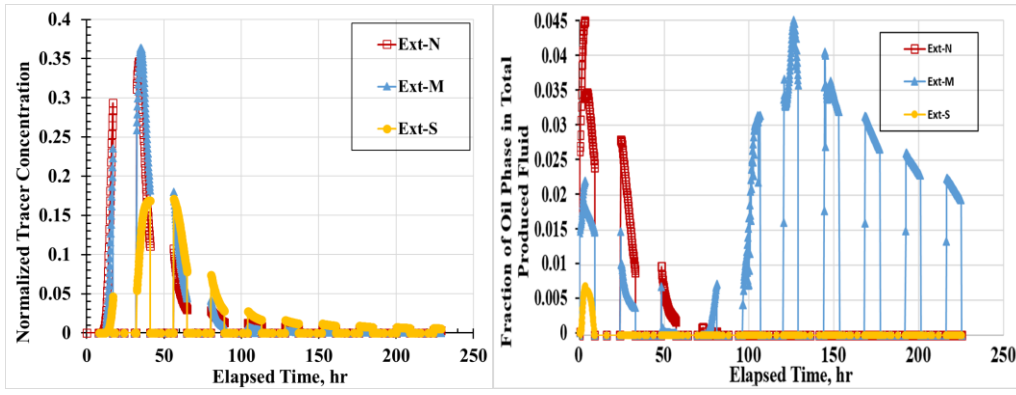


Figure 18. Change in oil saturation with time at three different layers (layer 1, 2, and 10) with oil density of 1.0 g/cc and viscosity of 0.7 cp (color scale showing oil saturation)



(a)

(b)

Figure 19. Tracer/surfactant-injection simulation results with oil density of 0.60 g/cc and viscosity of 0.7 cp: (a) effluent tracer concentration history and (b) effluent oil concentration history

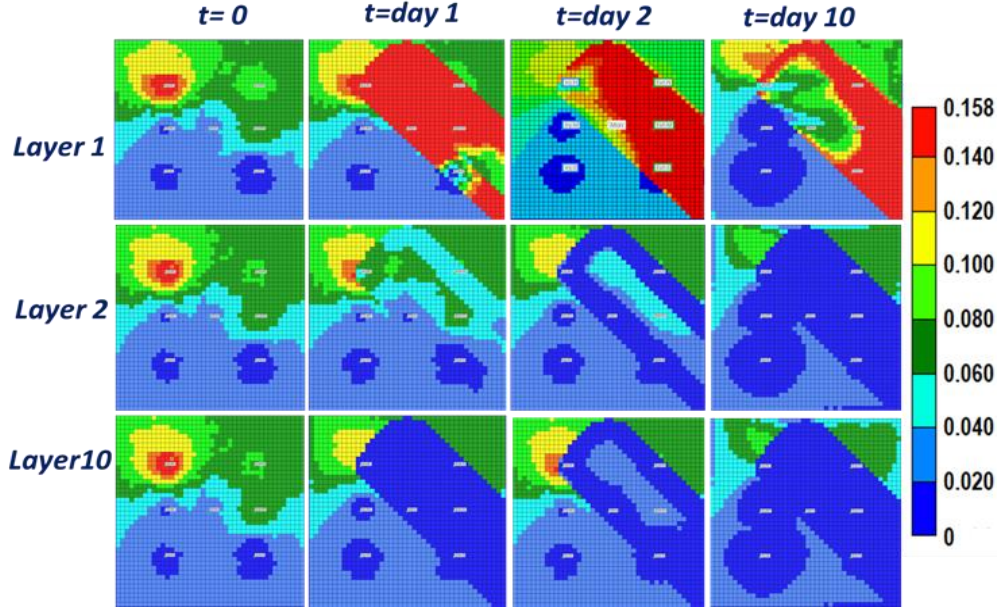


Figure 20. Change in oil saturation with time at three different layers (layer 1, 2, and 10) with oil density of 0.60 g/cc and viscosity of 0.7 cp (color scale showing oil saturation)

Part 4. Potential of follow-up foam processes

Given the level of heterogeneity in the system, this field can take advantage of surfactant/foam processes to overcome the subsurface permeability variations. The fact that surfactant solution is already injected helps the follow-up foam process by satisfying surfactant adsorption. This study considers another 10 days of gas-surfactant co-injection, or foam injection (in addition to the existing 10 days tracer/surfactant injection) at the same Q_t , but with $f_g = 80\%$ and $f_w = 20\%$ (or, $Q_w = 0.462 \text{ m}^3/\text{day}$ (surfactant solution) and $Q_g = 1.848 \text{ m}^3/\text{day}$ (air), equivalently). Mobility reduction factors (MRF) of 1, 10, and 100 are considered in order to

accommodate the reduction in the gas-phase mobility. Note that $MRF = 1$ represents the conventional gas-liquid two-phase flow with no foams, while $MRF = 10$ and 100 represent the cases of low-strength and high-strength foams, respectively.

Figs. 21 through 23 show how the process works when $MRF = 1, 10$ and 100 , respectively. When only gas and water are injected with no foam (Fig. 21), the injected fluids continuously displace the oil contaminants during those 10 days (i.e., Day 11 through Day 20). Compared to $MRF = 1$, foam injection with $MRF = 10$ and 100 (Figs. 22 and 23) shows more efficient displacement (i.e., higher oil production at earlier time with delayed breakthrough). More improvement is observed with higher MRF . This example proves the potential of foam application to follow in the field.

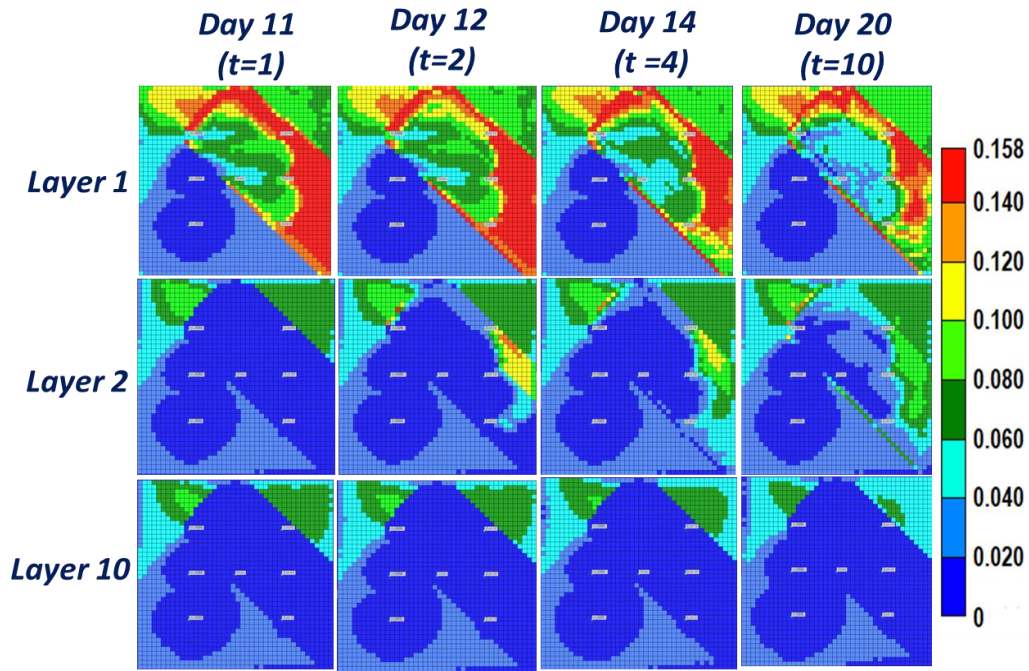


Figure 21. Change in oil saturation with time for potential follow-up foam injection at the same total injection rate with 80% gas fraction ($MRF = 1$, conventional gas-water injection (no foam) case) (color scale showing oil saturation)

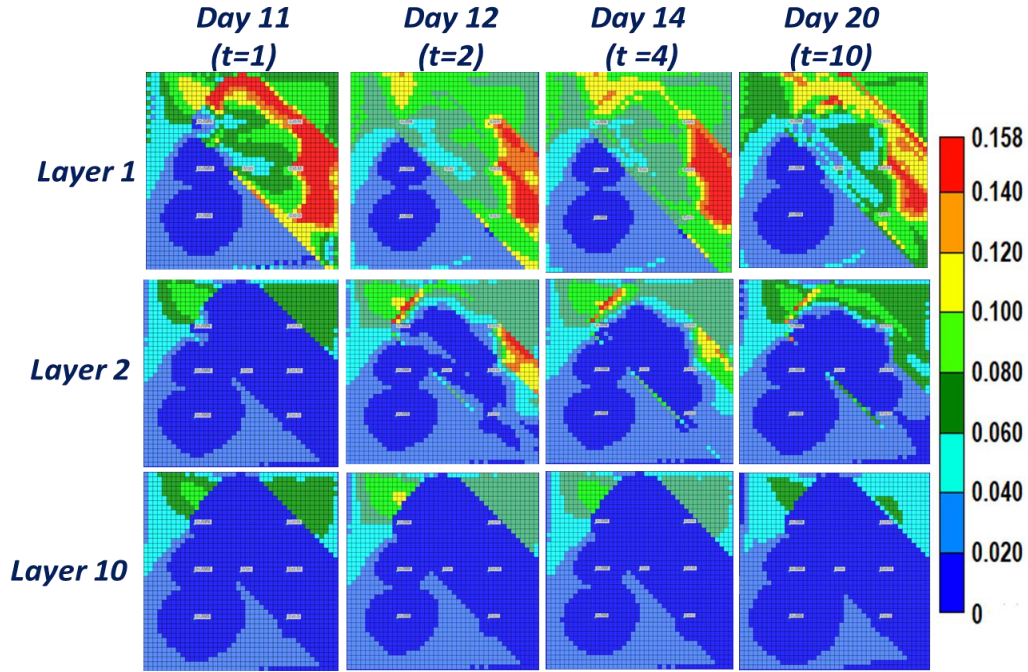


Figure 22. Change in oil saturation with time for potential follow-up foam injection at the same total injection rate with 80 % gas fraction (MRF= 10, low-strength-foam case) (color scale showing oil saturation)

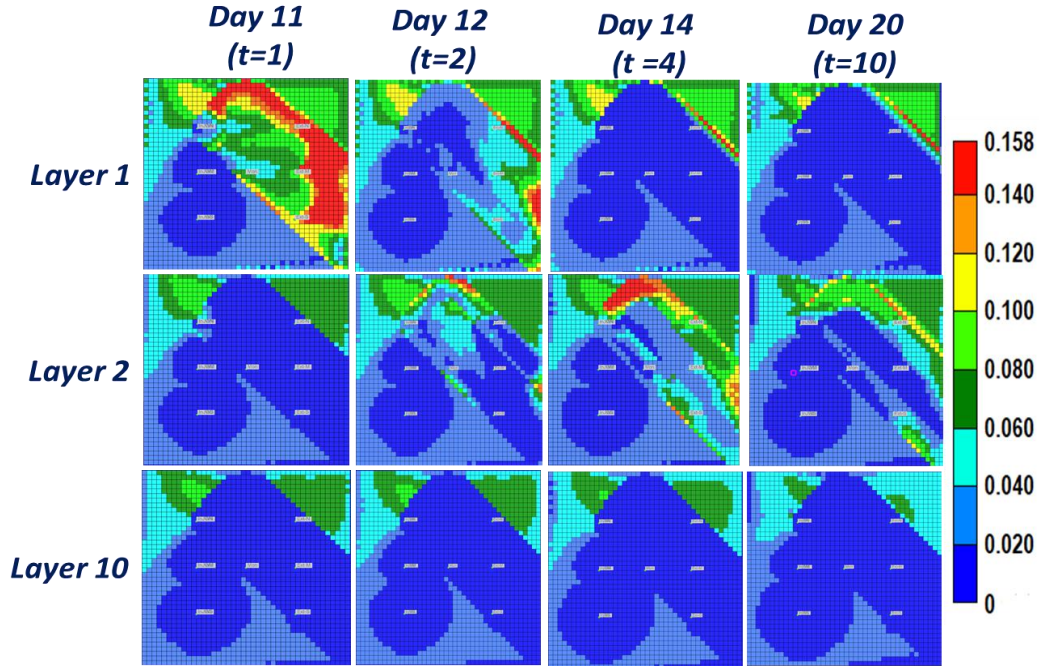


Figure 23. Change in oil saturation with time for potential follow-up foam injection at the same total injection rate with 80 % gas fraction (MRF= 100, high-strength-foam case) (color scale showing oil saturation)

Fig. 24 summarizes the simulation result, shown in Figs. 21 through 23, in terms of cumulative oil recovery, first 10 days of tracer/surfactant injection followed by next 10 days of foam injection. It clearly shows the benefit of injecting foams overcoming heterogeneity in subsurface remediation processes. Note that the amount of contaminants between the injection and extraction wells is about 0.327 m^3 ($5 \text{ m} \times 5 \text{ m} \times 3 \text{ m} \times 8.75 \% \times 0.05$). This means that the oil recovery at the end of 10-days surfactant injection is about 79.5 %, while the oil recovery at the end of additional 10-days foam injection is about 80.4, 85.0, and 89.6%, for MRF = 1, 10, and 100 respectively.

Actual foam field application, compared with history matching and future prediction by computer simulations, is designed as the next phase of this study.

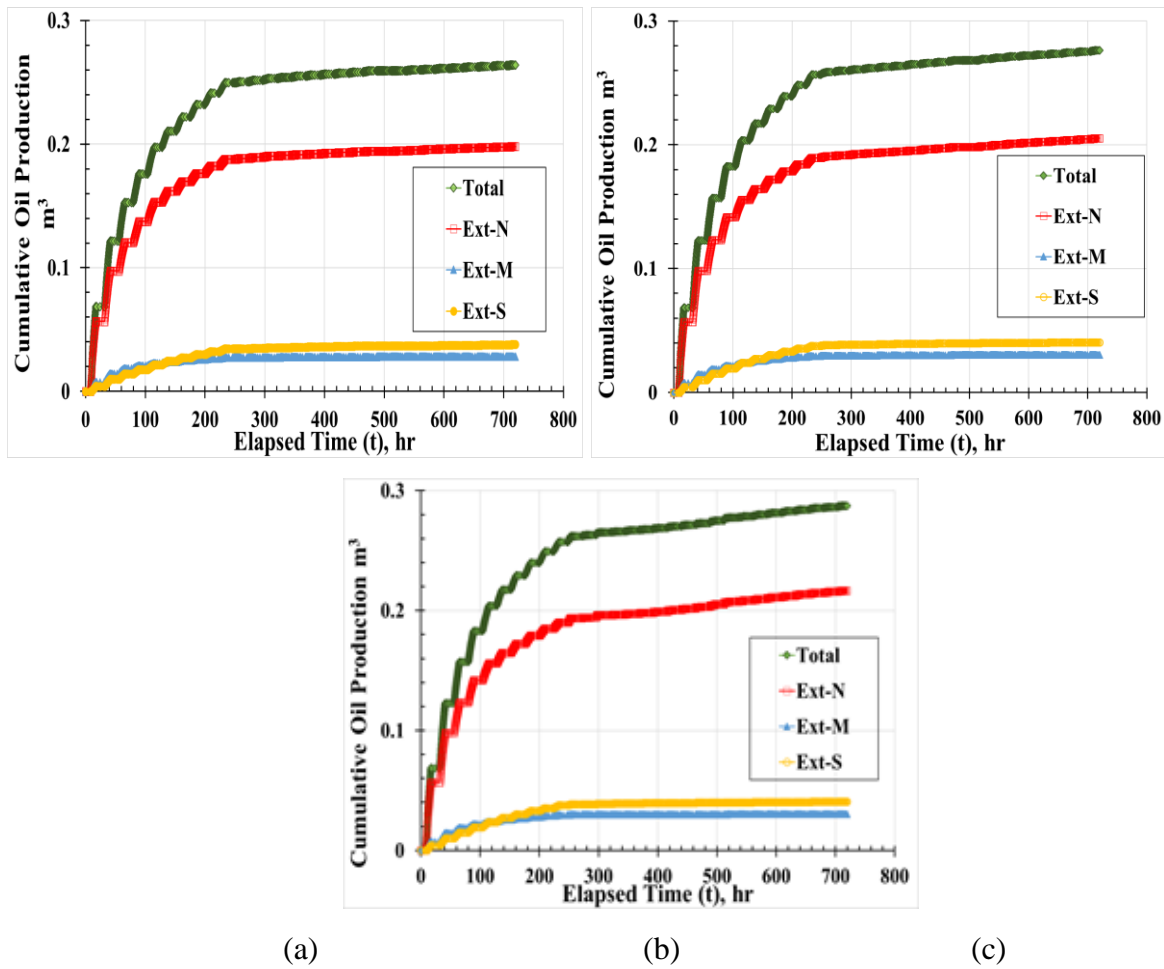


Figure 24. Oil production from individual wells during foam injection: (a) MRF = 1, (b) MRF = 10, and (c) MRF = 100

5. CONCLUSION

This study investigates a field application of tracer and surfactant injection processes, together with a possible follow-up foam remediation, performed within a military base in Si-Heung city, South Korea where the spill of non-aqueous phase liquid (NAPL) causes environmental and safety concerns. The specific site of interest, that is, about 5 m x 5 m area with 3 m depth of sands with high clay contents, is positioned below the foundation of fuel-distribution facility buildings.

When the simulation is carried out to match the production history of tracer concentration from three extraction wells (Ex-N, Ex-M, and Ex-S wells), the results imply that the site has a very high level of subsurface heterogeneity. The simulation with three permeability bands running from NW to SE reproduces the history of tracer production successfully. Such an anisotropic property coincides with the direction of groundwater flow from the field survey. The simulation also captures oil production history from the individual wells.

When the simulation is extended for future foam injection, it shows quite a promising outcome. With the ability of foams to reduce gas mobility, the sweep and displacement efficiencies are improved significantly such that the cumulative production of oil is enhanced at reduced operation time.

REFERENCES

- Abriola, L.M., Pennell, K.D., Pope, G.A., Dekker, T. J., Luning Prak, D. J.: Impact of Surfactant Flushing on the Solubilization and Mobilization of Dense Aqueous-Phase Liquid. In: Sabatini, D.A., Knox, R.C., Harwell, J.H. (eds.) Surfactant-enhanced subsurface remediation: Emerging technologies, ACS Symposium Series, vol. 594, pp. 10-23. Am. Chem. Soc., Washington, DC (1995). <https://doi.org/10.1021/bk-1995-0594.ch002>
- Abbaszadeh-Dehghani, M., Brigham, W.E.: Analysis of Well-to-Well Tracer Flow to Determine Reservoir Layering. J. Pet. Technol. 36, 1753-1762 (1984). <http://doi.org/10.2118/10760-PA>
- Alexandersen, D.K., Headley, T., Prigent, S., Mahmutoglu, I.: Ex-Situ Bioremediation of Hydrocarbon Contaminated Soil - An Example from Oman. Paper presented at the SPE Middle East Heal. Safety, Environ. Sustain Dev. Conf. Exhib, Doha, Qatar, 22-24 Sep 2014. <http://doi.org/10.2118/170411-MS>
- Alleman, B.C., Bedient, P.B., Borden, R.C.: Bioremediation of Chlorinated Solvent Plumes. In: Ward, C.H., Stroo, H.F. (eds.) In Situ Remediation of Chlorinated Solvent Plumes, pp. 309-318. Springer, New York (2010). <https://doi.org/10.1007/978-1-4419-1401-9>
- Chen, Z.: Reservoir Simulation: Mathematical Techniques in Oil Recovery. Soc. Ind. Appl. Math., Philadelphia, PA (2007)
- Cherry, J.A.: Groundwater Contamination by Petroleum Products. Paper presented at the 12th World Pet. Congr., Houston, Texas, 26 April 1987
- Ciocirlan, O., Iulian, O.: Density, Viscosity and Refractive Index of the Dimethyl Sulfoxide + xylene System. J. Serbi. Chem. Soc. 74, 317-329 (2009). <https://doi:10.2298/JSC0903317C.317>
- Cooke C.E., Jr.: Method of Determining Fluid Saturations in Reservoir. US Patent 3,590,923, 6 July 1971. <https://doi.org/10.1016/B978-075067785-1/50017-8>
- Descant, F., Blackwell, R., Pope, G.A., Sepehrnoori, K.: The Use of Single Well Tracer Testing To Estimate Heterogeneity. Unpublished Paper. Soc. Pet. Eng., (1989)
- Fetter, C.W.: Properties of Aquifers. In: Lynch, P., Hale, S., Sturla, B., (eds.) Applied Hydrogeology, pp. 66-112. Prentice-Hall, Upper Saddle River, New Jersey (2001)
- Gary, P.R.: NORM Contamination in the Petroleum Industry. J. Pet. Technol. 45, 12-16 (1993). <https://doi.org/10.2118/22880-PA>
- Jin, M., Delshad, M., Dwarakanath, V., McKinney, D. C., Pope, G. A., Sepehrnoori, K., Tilburg, C. E., Jackson, R. E.: Partitioning Tracer Test for Detection, Estimation, and Remediation Performance Assessment of Subsurface Non-aqueous Phase Liquids. Water Resour. Res. 31, 1201-1211 (1995). <http://doi.org/10.1029/95WR00174>
- Kam, S.I., Rossen, W.R.: A Model for Foam Generation in Homogeneous Media. Soc. Pet. Eng. J. 8, 417-425 (2003). <http://doi.org/10.2118/87334-PA>

- Lake, L. W., Johns, R. T., Rossen, W. R., Pope, G. A.: Enhanced Oil Recovery. Prentice Hall, USA (1989)
- Lee, S., Lee, G., Kam, S.I.: Three-Phase Fractional Flow Analysis for Foam-Assisted Non-Aqueous Phase Liquid (NAPL) Remediation. *Transport Porous Med.* 101, 373-400 (2014). <http://doi:10.1007/s11242-013-0250-y>
- Mamun, C.K., Rong, J.G., Kam, S.I., Liljestrand, H.M., Rossen, W.R. Simulating Use of Foam in Aquifer Remediation. In: Hassanizadeh, S.M., Schotting, R.J., Gray, W.G., Pinder, G.F. (eds.): *Developments Water Science*, vol. 47, pp. 867-874. Elsevier (2002). [https://doi.org/10.1016/S0167-5648\(02\)80152-6](https://doi.org/10.1016/S0167-5648(02)80152-6)
- McCarty, P.L.: Groundwater Contamination by Chlorinated Solvents: History, Remediation Technologies and Strategies. In: Ward, C.H., Stroo, H.F. (eds.) *In Situ Remediation of Chlorinated Solvent Plumes*, pp. 1-24. Springer, New York (2010). https://doi.org/10.1007/978-1-4419-1401-9_1
- Richter, W.: Experience in Oil and Gas Exploration and Exploitation with Regard to Groundwater Contamination and Groundwater Protection. Paper presented at the 7th World Pet. Congr. Mexico City, Mexico, 2-9 April, 1967
- Riser-Roberts, E.: Remediation of Petroleum Contaminated Soils: Biological, Physical, and Chemical Processes. Lewis, Boca Raton, FL (1998)
- Rosman, A., Kam, S.I.: Modeling Foam-Diversion Process Using Three-Phase Fractional Flow Analysis in a Layered System. *Energy Sources Part A.* 31, 936 – 955 (2009). <https://doi.org/10.1080/15567030701752875>
- Roostapour, A., Lee, G., Zhong, L., Kam, S.I.: Model Fit to Experimental Data for Foam-Assisted Deep Vadose Zone Remediation. *J. Hazard. Mater.* 264, 460-473 (2014). <https://doi.org/10.1016/j.jhazmat.2013.09.016>
- Roostapour, A., Kam, S.I.: Modeling Foam Delivery Mechanisms in Deep Vadose-zone Remediation Using Method of Characteristics. *J. Hazard. Mater.* 243, 37-51 (2012). <https://doi.org/10.1016/j.jhazmat.2012.09.014>
- Shackelford, C.D., Jefferis, S.A.: *Geoenvironmental Engineering for in Situ Remediation*. Paper presented at GeoEng. Melbourne, Australia, 19-24 Nov, 2000
- Simpkin, T.J., Sale, T., Kueper, B.H., Pitts, M.J., Wyatt, K.: Surfactant/Cosolvent Enhanced Recovery of NAPL. In: Lowe, D.F., Oubre, C.L., Ward, C.H. (eds.) *Surfactants and Cosolvents for NAPL Remediation*, pp. 41-88. Lewis, Boca Raton, FL (1999)
- Szafranski, R., Lawson, J.B., Hirasaki, G.J., Miller, C.A., Akiya, N., King, S., Jackson, R.E., Meinardus, H., Londergan, J.: Surfactant/foam Process for Improved Efficiency of Aquifer Remediation. In: Rehage H., Peschel, G. (eds.) *Structure, Dynamics and Properties of Disperse Colloidal Systems*. *Prog. Colloid Polym. Sci.*, vol. 111, pp.162-167. Springer, Heidelberg (1998). <https://doi.org/10.1007/bfb0118126>

- Tang, J.S.: Partitioning Tracers and In-Situ Fluid Saturation Measurements. SPE Form. Eval. J. 10, 33-39 (1995). <https://doi.org/10.2118/22344-PA>
- Um, J., Lee, G., Song, S., Hong, S., Lee, M.: Pilot Scale Feasibility Test of In-situ Soil Flushing by Using 'Tween 80' Solution at Low Concentration for the Xylene Contaminated Site. J. Soil Groundw. Environ. 18, 38-47 (2013). <https://doi.org/10.7857/JSGE.2013.18.6.038>
- Zhong, L., Oostrom, M., Truex, M.J., Vermeul, V.R., Szecsody, J.E.: Rheological Behavior of Xanthan Gum Solution Related to Shear Thinning Fluid Delivery for Subsurface Remediation. J. Hazard. Mater. 244-245, 160-170 (2013). <https://doi.org/10.1016/j.jhazmat.2012.11.028>

VITA

Hazem Fleifel is from Damascus, Syria. He received his bachelor degree in Geophysics with a minor in Geology from Damascus University in May 2013. He worked at ExxonMobil, Baton Rouge and Dow, Plaquemine doing refinery maintenance from 2016 to 2017.

In 2018, he joined the Craft and Hawkins Department of Petroleum Engineering at Louisiana State University as an M.S. candidate in the Fluid Mechanics and Foam Injection EOR research group led by Dr. Seung Ihl Kam. During his time at Louisiana State University he held different assignments such as Student Worker at the Petroleum Engineering Research & Technology Transfer Laboratory (PERTT Lab), Supplement Instructor for Rock Properties, and Teaching Assistant for two courses: Rock Properties Lab and Numerical Simulation of Improved Recovery Processes. He plans to graduate May 2020.